From fabric to tissue: Recovered wool keratin/polyvinylpyrrolidone biocomposite fibers as artificial scaffold platform

From fabric to tissue: recovered wool keratin/polyvinylpyrrolidone biocomposite fibers as artificial scaffold platform

Giulia Suarato[a,b,], Marco Contardi[a], Giovanni Perotto[a], Jose' A. Heredia-Guerrero[a], Fabrizio Fiorentini[a], Luca Ceseracciu[c], Cataldo Pignatelli[a], Doriana Debellis[d], Rosalia Bertorelli[b], Athanassia Athanassiou[a,*]*

[a] Smart Materials, Istituto Italiano di Tecnologia, Via Morego, 30, Genova 16163, Italy

[b] Translational Pharmacology, Istituto Italiano di Tecnologia, Via Morego, 30, Genova 16163, Italy

[c] Materials Characterization Facility, Istituto Italiano di Tecnologia, Via Morego, 30, Genova 16163, Italy

[d] Electron Microscopy Facility, Istituto Italiano di Tecnologia, Via Morego, 30, Genova 16163, Italy

Abstract

Keratin extracted from wool fibers has recently gained attention as an abundant source of renewable, biocompatible material for tissue engineering and drug delivery applications. However, keratin extraction and processing generally require a copious use of chemicals, not only bearing consequences for the environment but also possibly compromising the envisioned biological outcome. In this study, we present, for the first time, keratin-PVP biocomposite fibers obtained via an all-water co-electrospinng process and explored their properties modulation as a result of different thermal crosslinking treatments. The protein-based fibers featured homogenous morphologies and average diameters in the range of 170 – 290 nm. The thermomechanical stability and response to a wet environment can be tuned by acting on the curing time; this can be achieved without affecting the 3D fibrous network nor the intrinsic hydrophilic behavior of the material. More interestingly, our protein-based membranes treated at 170 °C for 18 h successfully sustained the attachment and growth of primary human dermal fibroblasts, a cellular model which can recapitulate more faithfully the physiological human tissue conditions. Our proposed approach can be viewed as pivotal in designing tunable protein-based scaffolds for the next generation of skin tissue growth devices.

Keywords: Wool keratin, Polyvinylpyrrolidone, Biocomposite fibers, Waste reuse, Wound healing

1. Introduction

Considerable interest of the biomedical community has been drawn towards the quest for eco-friendly, biocompatible and biodegradable materials, either derived from natural resources or obtained as secondary raw materials from industrial production, biomasses or agriculture. The use of these renewable resources together with the implementation of sustainable production processes may represent valuable alternative in reducing environmental pollution and preserving non-renewable natural resources. Moreover, thanks to their unique properties, naturally-derived materials constitute a promising platform to develop innovative, functional biocomposites.[1,2] Due to the versatile nature of the polypeptide macromolecules, proteins have rose as relevant candidates. Amongst them, keratin constitutes one of the most abundant, that can be found in the epithelial cells of mammals, birds and reptiles, as a structural component of hair, nails, wool, feathers and horns.[3] Nowadays, keratin waste from wool textile industry, slaughter houses, poultry farming, and hair salons has been estimated to reach 40 million tons per year.[3] However, the current standards for disposal, landfill and burning procedures, pose high environmental risks since they call for abnormal sulfide release.[4–6] Therefore, alternative applications for the large amount of unused or discarded keratins are deeply sought.

Wool keratin is composed of low-sulfur intermediate filaments (40 – 65 kDa, about 60% of the wool fiber) mostly presenting an α-helical structure, embedded in an amorphous matrix which comprises high-sulfur fractions (11 – 25 kDa, γ-keratins, about 30% of the wool fiber) and high-tyrosine/glycine proteins (6 – 9 kDa, about 12% of the wool fiber).[3,7,8] β-keratins form the outer cuticle, and serve a protective function. Being rich in cysteine residues, the cortical structure is tightly kept together by disulfide linkages.[9] To degrade the disulfide bonds, several extraction protocols have been proposed, either based on chemical reactions (*i.e.* reduction[10] via thiols or

oxidation with peracetic acid), physical methods (*i.e.* steam explosion[11], microwave irradiation[12]) or green-chemistry approaches (*e.g.* ionic liquids[13], cysteine reduction[14], and hydrolysis via microbial digestion[15]). Each method would allow to isolate specific fractions of the polypeptide chains for further transformation, characterized by a range of molecular weights and presenting different aminoacidic residues (*e.g.* cysteine or sulfonic acid, amino acids with polar side groups), suitable for a distinct application.[16,17]

In the past decades, keratin has gained attention as functional material for various applications in the biomedical field. Porous sponges based on human hair or wool extracted keratin have been investigated *in vitro*[18–20], and examined *in vivo* for tissue inflammation or integration[9,21] and wound closure capability.[22–25] The remarkable findings on the cellular – matrix interaction have been ascribed to the presence of specific amino acid sequences, such as arginine – glycine – aspartic acid (RGD) and leucine – aspartic acid – valine (LDV), present in various keratin proteins. These sequences hold a pivotal role in eliciting the signaling cascade involved in promoting cell adhesion and tissue regeneration.[19] In previous studies, lyophilized sponges of human hair keratin were investigated as substrates for the growth of NIH3T3 mice fibroblasts,[19] while L929 cells were cultivated long-term onto wool-extracted keratin coatings.[26] More recently, human hair keratin / fibroin composite membranes have been proposed as vascular tissue reconstruction platform,[27] while Sierpinski *et al.* successfully cultured Swann cells onto human hair keratin hydrogels for peripheral nerve regeneration,[28] suggesting the great potentiality of this protein-based biomaterial. In addition, keratin biomaterials have shown hemostatic and anti-inflammatory properties.[29] Moreover, keratin has been proposed as building block for controlled drugs / active molecules delivery systems in diverse formulations, such as films[30], hydrogels[5,16,31–33], electrospun fibers[34,35], and microparticles.[36] This versatility in the design suggests further potentialities of this natural

material in tuning the crucial features involved in the regulation of cell-material interactions (*i.e.* biodegradation rate and morphological structure). However, due to the rather low molecular weight (10 – 60 kDa), poor viscoelastic properties, and limited mechanical stability, the fabrication of keratin nanofibers via electrospinning is rather challenging, and the process is usually carried out in the presence of organic solvents, such as formic acid[17] and hexafluoro-isopropanol.[37,38] To overcome the spinnability issues and support the fiber formation process, adjuvant polymers are unavoidable, and a plethora of them has been proposed in the literature, *i.e.* PEO[6,39], PVA[40,41], synthetic polyesters (PLLA[42] and PCL[43–45]), and natural polymers (PHBV[37] and fibroin[27]).

In the present study, we combined, for the first time, wool keratin with polyvinylpyrrolidone (PVP), a biocompatible polymer[46–48] with higher molecular weight that allowed the fabrication of homogeneous nanofibers from an all-water based electrospinning approach. The protein was extracted from discarded wool (industrial waste) with a low-surfactant assisted reduction process. With the aim of designing a scaffold suitable for skin growth, a thermal crosslink of the fibrous matrices was developed to prevent fast dissolution of the material. The thermal curing was preferred over the use of chemical crosslinking strategies[39,49] thus minimizing the release of compounds potentially harmful for the envisioned biological application. The thermally treated biocomposite membranes were characterized in terms of their morphology, chemical modifications, thermomechanical behavior, and response to enzymatic degradation. Finally, primary human dermal fibroblasts and human epidermal keratinocytes were used to evaluate the Ker-PVP fiber cytocompatibility *in vitro* with via MTS assay, while adhesion studies confirmed the suitability of the recovered protein-based network as provisional extracellular matrix.

2. Experimental

2.1 Materials

Argentinian sheep wool was kindly donated by Olimpias s.r.l. (Ponzano Veneto, TV, Italy). β-Mercaptoethanol (βME), dithiothreitol (DTT), thioglycolic acid (TGA), sodium metabisulfite, tris(2-carboxyethyl) phosphine (TCEP), polyvinylpyrrolidone (PVP; M_W ~ 1,300,000 Da), methanol, acetone, sodium dodecyl sulphate (SDS), Trizma® base (Tris), and chloride acid were purchased from Sigma-Aldrich. Laemmli Sample Buffer, Precision Plus Protein™ All Blue Prestained Protein Standards (marker), 40% acrylamide/bis solution, ammonium persulfate (APS), tetramethylethylenediamine (TEMED), Coomassie staining and destaining solutions were purchased from Bio-Rad. Glutaraldehyde, ethanol, hexamethyldisilazane, osmium tetroxide and cacodylate buffer were purchased from Sigma-Aldrich. Deionized water was obtained from Milli-Q Advantage A10 ultrapure water purification system.

2.2 Wool keratin extraction

Raw wool fibers were washed in a 1:1 solution of acetone:methanol for at least 6 h under mild agitation. Fibers were thoroughly washed with MilliQ water and let dry overnight at room temperature. Extractions of keratin from wool were performed with 2 g of washed wool fibers in in a 7 M urea solution (36 mL) with or without SDS (0.107 M) and using five different reduction agents to reduce the disulfur bridge of the cysteine: β-mercaptoethanol (βME – 1.2 M), dithiothreitol (DTT – 0.1 M)[10], thioglycolic acid (TGA – 1.2 M)[50,51], sodium metabisulfite ($NaHSO_3$ – 0.93 M, in 67 mL of 7 M urea)[52], and Tris(2-carboxyethyl) phosphine (TCEP – 1.2 M). In addition, to assess the effect of the protein denaturing agent on the extraction yield, different concentrations of SDS were considered (from 0.0125 to 0.107 M), while the reducing compound (βME – 1.2 M) was kept constant.

For each extraction experiment, the washed wool fibers were immersed in the reagent mixtures and heated at 60 °C for 4 h in an oven. The fibers were filtered through a 40-mesh stainless steel grid to separate the dissolved keratin from the undissolved fibers. The extracted keratin was dialyzed against distilled water for 48 h, by means of dialysis tubes (M_w cut off of 3500 Da, SpectrumLabs). The dialyzed keratin (Ker) was then centrifuged (three times, at 9000 rpm and 4 °C for 20 minutes), to eliminate residues and fibrous debris, and finally stored at 4 °C up to a month. To measure the concentration of each batch of extraction, 1 mL of protein solution was let drying on a weighting cup and the amount of regenerated protein was calculated from the weight difference. In addition, the process yield was calculated according to equation (1):

$$Yield = \frac{mass\ extracted\ in\ solution\ (gr)}{starting\ wool\ (gr)} * 100\% \qquad eq.\ (1)$$

2.3 SDS-Page electrophoresis

To characterize the extracts from wool, SDS-page electrophoresis was performed. SDS–PAGE, 12% (w/v) polyacrylamide separating gel and 4% w/v polyacrylamide stacking gel were used to resolve proteins at 80 V for 30 minutes and at 120 V for 60 minutes. A wide-range molecular weight (15–250 kDa) marker was run along with the proteins. Extracts from wool (30 µg) were added to an appropriate volume of Laemmli Sample buffer with 50 mM dithiothreitol (DTT) and heated at 75 °C for 10 minutes, in order to induce denaturation of the protein samples. The gel was colored with Coomassie Brilliant Blue R-250 0.1% in a mixture of methanol:acetic acid:water (40:10:50, in volume) for 30 minutes, and decolored in methanol:acetic acid:water (20:10:70, in volume) overnight.

2.4 Keratin:PVP fibers fabrication and thermal treatment

The biocomposite fibers were prepared by adding PVP powder in the extracted keratin water solutions, at a weight ratio of 1:3 (Ker:PVP, w/w). An example of the component

concentrations in the electrospinning solution is reported as follows. For a recovered wool keratin solution of 19 mg/mL of concentration (batch-to-batch dependent), 5 mL contain 95 mg of keratin. In order to favor the spinnability process, 285 mg of powder PVP are added into the water-keratin solution, leading to a resulting synthetic polymer concentration of 57 mg/mL. The system was kept under gentle shaking for 18 h, to allow for complete polymer dissolution and homogenous dispersion within the protein solution. Fibrous mats were obtained with an electrospinning setup comprising of a syringe pump (NE-1000, New Era Pump Systems, Inc.), working at constant flow rate of 600 μL/h. The spinneret (stainless-steel, 18-gauge) was clamped to a positive electrode connected to a power supply (generating 18 kV), while an Aluminum disk placed at a distance of 20 cm from the needle tip was used as collector. Afterwards, the obtained fibers were removed from the Aluminum disk and oven-treated at 170 °C for different amount of time (30 minutes, 1, 3, 5, 18, and 24 h).

2.5 Morphological characterization

The morphology of the fibers was characterized by scanning electron microscopy (SEM), using a SEM JEOL-JSM 6490 operating with an acceleration voltage of 10 kV. The specimens were coated with a 10 nm thick film of gold using a Cressington Sputter Coater – 208 HR. The diameters of the fibers and the matrices porosity were analyzed via ImageJ software[53] (https://imagej.nih.gov): for each sample, about 250 measurements were taken to evaluate the average diameter distribution of the fibers, and 5 images (range of magnification 5000*X* and 12000*X*) were processed for the porosity estimation. The pore dimensions were estimated assuming a circular geometry, while the samples porosity was evaluated as percentage of the total image area. Data are presented as averages ± standard deviations.

2.6 ATR-FTIR analysis

Infrared spectra were obtained with a single-reflection attenuated total reflection (ATR) accessory *(MIRacle* ATR, PIKE Technologies) equipped with a diamond crystal and coupled to a Fourier Transform Infrared (FTIR) spectrometer (Equinox 70 FT-IR, Bruker). All spectra were recorded in the range from 3800 to 600 cm^{-1} with a resolution of 4 cm^{-1}, accumulating 128 scans.

2.7 Thermal characterization

The thermal degradation behavior of the biocomposite fibers was investigated by a standard thermogravimetric analysis (TGA) method with a TGA Q500 from TA Instruments. About 3–5 mg samples were placed in an Aluminum pan, in an air-containing atmosphere with a flow rate of 50 mL/min. A Temperature range from 30 to 600 °C with a heating rate of 5 °C/min was used. The weight loss and its first derivative were recorded simultaneously as a function of time/temperature.

2. 8 Mechanical characterization

Mechanical properties of the electrospun Ker-PVP biocomposite fibers, as a function of the thermal treatment time, were characterized by uniaxial tension on a dynamometer (Instron 3365) equipped with a 10 N load cell. Briefly, samples (25 mm length, 5 mm width) were first mounted on paper frames for ease of handling and gripping. The two halves of the frame were then separated prior to testing. Load was applied with the rate of 1 mm/min until failure. From the stress-strain curves, the Young's modulus *E*, ultimate tensile stress *UTS* and elongation at break ε_r were extracted.

2.9 Water absorption

Water absorption capacity of the fibrous samples was obtained as follow. Five dry samples were weighed on an electronic balance with 0.01 mg sensitivity and then placed in different

chambers with controlled, increasing humidity (0%, 11%, 44%, 84%, and 100%). In order to obtain the desired humidity conditions, saturated aqueous solutions were prepared as follows: (a) Lithium Chloride (42 M) for the 11% H.R.; (b) Potassium Carbonate (16 M) for the 44% H.R.; (c) Potassium Chloride (33 M) for the 84% H.R. To maintain a completely dry atmosphere (0% H.R.), the chamber was conditioned with anhydrous silica gel beads, while MilliQ water was used to saturate the chamber at 100% H.R. Before performing the experiment, the samples were dried in a desiccator until no change in sample weight was measured. After conditioning in different humidity chambers until equilibrium conditions, each sample was weighed, and the amount of absorbed water was calculated as difference from the initial, dry weight.

2.10 Contact angle

Water contact angle measurements were obtained via an optical contact angle measuring instrument (Dataphysics OCAH200) with 5 μL deionized water droplets. Self-standing fibrous matrices (average thickness of 450 μm ca.) were cut into round pieces with a puncher (12 mm in diameter) and attached onto a glass slide with double-sided tape to ensure sample planarity. At least 10 repetitions were acquired for each condition.

2.11 Water stability

Ker-PVP fibrous samples, either pristine or thermally treated, were cut in small pieces in order to fit onto 13-mm glass coverslips placed in the wells of a 24-well plate. Two and a half mL of PBS (pH 7.4) were placed in each well, in order to completely immerse the fibers. After 24 h at room temperature, the samples were retrieved, dried and imaged under the SEM (SEM JEOL-JSM 6490) using the above-mentioned parameters.

To characterize the effect of the enzymatic degradation, the thermally treated Ker-PVP fibers that resulted stable in a water environment were cut in small pieces, weighted, and

individually inserted in the wells of a 24-well plate. Each sample was kept in 3 mL of Protease XIV from *Streptomyces griseus* (≧ 3.5 units/mg, Sigma Aldrich) in PBS (pH 7.4, 4 U/mL) and incubated at 37 °C for 14 days. At fixed time points (1, 3, 5, 7, and 14 days), the samples were withdrawn, oven dried at 50 °C for 72 h to allow for a complete desiccation, and finally weighted. The weight loss was calculated as difference from the initial, dry weight. At each time point, a reference sample was sputter-coated with 10 nm of Au and SEM images were acquired using a SEM JEOL-JSM 6490 operating with an acceleration voltage of 5 kV.

2.12 In vitro biocompatibility assay of the Ker-PVP fibers extract

Primary human dermal fibroblasts adult (HDFa, Thermo Fisher Scientific) and primary human epidermal keratinocytes adult (HEKa, Thermo Fisher Scientific) were used to investigate the biocompatibility of the Ker-PVP biocomposite fibers. Cells were cultured in T75 culture flasks with either Medium 106 (Thermo Fisher Scientific) supplemented with LSGS Kit (for HDFa cells) or with Medium 154 (Thermo Fisher Scientific) supplemented with KKGS Kit (for HEKa cells), in an incubator at 37 °C and with 5% CO_2. HDFa cells were seeded onto 24-well plates at a density of 7000 cells/cm^2, while HEKa cells were plated onto 96-well plates at a density of 14000 cells/cm^2 and let attach overnight. Extraction medium from the fibrous samples were prepared in accordance to the ISO10993-5:2009 standard test. Briefly, the fibrous samples (Ker-PVP fibers kept at 170 °C for 18 h) were cut into 6 cm^2 – pieces and sterilized under ultraviolet light for 30 min (15 min per side). Afterwards, the samples were covered with 1 mL of cell culture medium for 24 h at 37 °C. Attached cells were then treated with the extraction media and incubated for 24 h, while cells incubated in normal Medium were considered as controls. Cell viability was determined via MTS assay (tetrazolium salt, CellTiter 96®AQ_{ueous} One Solution Cell Proliferation Assay, Promega). Prior to adding the reagent, the extraction media was replaced with fresh culture media, to avoid

alterations during the readings due to uneven liquid evaporation. Samples were kept in a humidified incubator at 37 °C and with 5% CO_2 for additional 3.5 h. Absorbance readings of the optical density at 490 nm were recorded. In Figure S1 a schematic representation of the *in vitro* biocompatibility assay is reported. Three independent experiments were carried out, each with triplicates, and results are herein reported as mean ± standard error. A Student's *t*-test, assuming unequal variances, was carried out, considering a $p < 0.01$ value.

In order to visualize the morphology of the cells exposed to the Ker-PVP fiber extracts, fibroblasts were plated onto glass coverslips at a density of 7000 cells/cm^2 and treated as above-mentioned. Afterwards, the samples were washed with pre-warmed PBS (pH 7.4) and fixed with 3.7% paraformaldehyde (PFA) for 20 minutes. Nuclei staining was obtained by incubation in a DAPI solution (2.5 μg/mL) for 15 minutes in the dark, followed by two washing with PBS. To allow the cytoskeleton actin staining, samples were permeabilized with 0.3% Triton X-100 for 8 minutes and washed 2 times with PBS, prior to incubation in Alexa Fluor 488 Phalloidin (Thermo Fisher Scientific, 1:100 dilutions in PBS) for 20 minutes in the dark. Stained coverslips were then mounted with Fluoromont-G onto glass slides and imaged with a confocal microscope Nikon A1, equipped with 405 and 488 lasers.

2.13 Cell plating onto the Ker-PVP fibrous scaffold

Ker-PVP biocomposite fibers (kept at 170 °C for 18 h) were cut in circular shapes in order to fit onto 13-mm glass coverslips and sterilized under ultraviolet light for 30 min (15 min per side). Afterwards, a PDMS ring was inserted in each well, to prevent the fibrous matrix from floating during the experiment. Primary human dermal fibroblasts adult at 80% confluency were trypsinized and seeded at a density of 5000 cells/cm^2. Cells were let attach and grow onto the fibrous network for 72 h in a humidified incubator at 37 °C and with 5% CO_2. Afterwards, samples

were washed with pre-warmed PBS (pH 7.4) and fixed with 3.7% paraformaldehyde (PFA) for 20 minutes. In order to avoid the unspecific adsorption of the dyes to the protein-PVP fibers, all the staining solutions were prepared in 1% Bovine Serum Albumin (BSA). The nuclei staining was obtained with DAPI (2.5 μg/mL in BSA, 15 minutes in the dark). To allow the cytoskeleton actin staining, samples underwent permeabilization with 0.3% Triton X-100 for 8 minutes, prior to incubation in Alexa Fluor 488 Phalloidin (1:100 dilutions in BSA) for 20 minutes in the dark. The stained fibrous samples were carefully removed from the wells and gently sandwiched with Fluoromont-G between a glass slide and a squared coverslip. The samples were imaged with a confocal microscope Nikon A1, equipped with a 560 nm laser. Images were acquired with both PMT and spectral detector, under a Plan Apo 20x DIC.MN2 optics, with a NA of 0.75. The spectral acquisition ranged from 567.7 nm to 740.6 nm, with a grating resolution of 6 nm. The image analysis (spectral unmixing, ROI definition and spectral profiling) was carried out with ImageJ[53] (https://imagej.nih.gov).

2.14 SEM imaging of the Ker-PVP fibrous scaffolds

Ker-PVP fibrous scaffolds (kept at 170 °C for 18 h), prepared as above-mentioned and seeded with HDFa cells for 72 days, were fixed in a solution of 2% glutaraldehyde in 0.1 M cacodylate buffer for 2 h at room temperature. After several washes in the same buffer, the samples were post-fixed in osmium tetroxide (1% in MilliQ water) for 2 h and washed with MilliQ water. Subsequently, the scaffolds were dehydrated with a series of incubations in increasing concentrations of ethanol in water solutions (from 30% to 100%, 10 minutes each), followed by incubation in 1:1 ethanol:hexamethyldisilazane (HMDS, Sigma-Aldrich) and 100% HMDS. Lastly, the samples were dried overnight in air and sputtered with a 10 nm gold layer. Imaging

analysis was performed using a JEOL JSM-6490LA Scanning Electron Microscope equipped with a tungsten filament and operating at 10 KV of accelerating voltage.

3. Results and Discussion

3.1 Extraction protocol optimization

Keratin molecules stability is strongly associated with the presence of intramolecular disulfide bonds. Many are the strategies implemented to cleave these linkages, either based on chemical reactions or physical methods. Recently, efforts have been attempted in proposing new, eco-friendly methods for the extraction of keratin from human hair and other animal sources.[14,54,55]

In our study, βME was identified as the preferred thiol-containing reducing agent to break the disulfide bonds and form cysteine residues (Figure 1a), after a preliminary experiment were various extraction protocols were considered (Figure S2). The denaturing agent urea, usually included to weaken the hydrophobic intramolecular interactions and facilitate the βME action[14], was used at a fixed concentration of 7 M. In an effort of limiting the amount of potentially harmful reagents while keeping optimal the extraction efficiency, a spectrum of SDS molarity was tested. As keratins tend to aggregate and oxidize during dialysis (when both urea and βME are washed away), the surfactant molecules complex with the polypeptide chains helping their solvation and stability in water.[55] In fact, by disrupting the coiled conformation and interacting with the hydrophobic domains of the protein, the surfactant allows the hydrophilic pockets to be exposed to the water environment, thus limiting the intra-chain entanglements.[55]

The effects of the surfactant content in the reaction bath on the molecular weight (Mw) of the recovered protein fractions and on both the overall protein concentration and yield extraction were investigated. From the SDS-PAGE in Figure 1b, two main bands are visible around 37 and

above 50 kDa, proper of the intermediate filaments, the structural α-keratins. Bands between 8 and 15 kDa are associated with the fractions rich in glycine and tyrosine content, while the opaque contributions between 15 and 25 kDa indicate the so-called "high sulfur" matrix protein, the γ-keratins.[3,56] The lower the SDS within the mixture, lower the content of α-keratins recovered, as the reducing agent was not able to completely react with the poorly solvated protein molecules. In parallel, the resulting extraction yields and material concentrations (Figure 1c) levelled down when a low SDS molarity was added. The best conditions were set between 0.05 and 0.075 M, where fair concentrations (in the range of 17.5 and 19 mg/mL) and good process turnouts of (55.5 ± 0.1) % and (68.7 ± 0.3) % were achieved, respectively (Table S1). The small yield increments observed with the highest amount of surfactant (0.107 M) did not compensate for the rather "soapy" aspect of the solution. When the SDS was completely removed from the system (Figure S2) the protein partly precipitated during the dialysis, leading to a flocculant dispersion.

The recovered, dialyzed protein solution, mostly consisting of structural α-keratins, was used to fabricate non-woven matrices via an all-water electrospinning process.

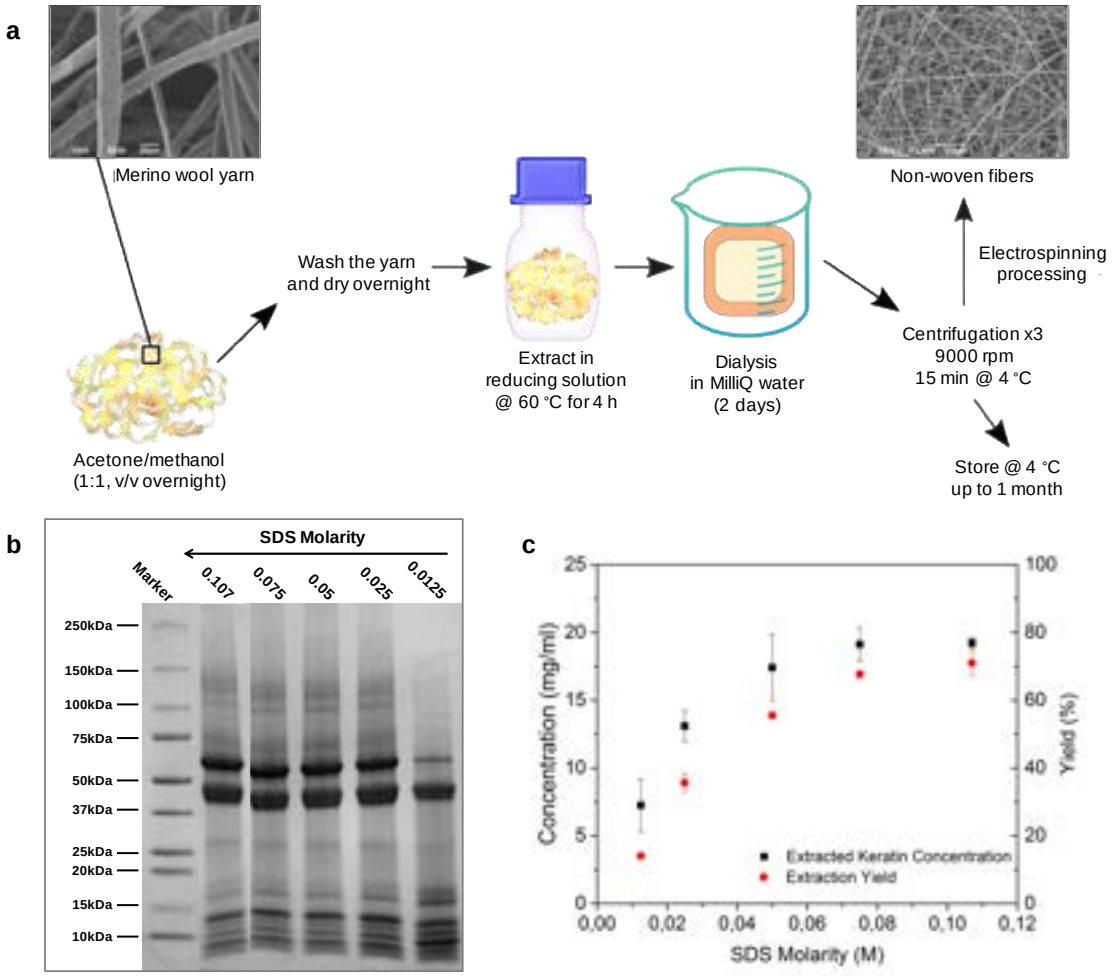

Figure 1. Keratin proteins are extracted from Merino wool by means of reducing agents. (a) Schematic depicting the general extraction protocol; (b) effect of the SDS molarity on the type of keratins extracted; (c) effect of the SDS molarity on the keratins' final concentration and process yield.

3.2 Morphological characterization of the electrospun matrices

Due to the typically low molecular weights (in the range of 10 – 60 kDa) which characterize their various fractions, keratins are often processed either in combination with other polymers[6,39,40,43,57] or starting from acidic solutions.[17] In our study, keratin-based nanofibers were obtained via an all-water, eco-friendly electrospinning process by incorporating for the first time polyvinylpyrrolidone as an adjuvant into the protein solution. The addition of this biocompatible and biodegradable, high Mw polymer increased the composite solution viscosity, thus endowing it with spinnability under the applied electric field. The nanofibers, homogeneously deposited onto the grounded target under a continuous jet, presented uniform morphology and quite monodispersed size distribution (Figure 2a-c).

With the aim of fabricating protein-based scaffolds able to sustain skin cells growth, immediate dissolution upon contact with water needs to be avoided. To delay the matrix solubility, confer mechanical stability, and improve the overall storage life, fibers were thermally treated at 170 °C for different treatment durations. In Figure 2d-n and Table 1, the morphology and the size distribution for the fibers treated for 30 minutes, 5 h, and 18 h are presented (while in Figure S3 and Table S2 results for fibers subjected to oven-treatments of 1, 3 and 24 h are considered). The strategy of the thermal treatment was preferred over the conventional crosslinking with formaldehyde vapors,[52] glutaraldehyde solution,[49] genipin or metal complexes,[7] given the high toxicity of these chemicals which would diverge from our green fabrication standards and might interfere with the final biological application. Moreover, Aluigi *et al.*[17] proposed the use of high temperature (180 °C for 2 h) to favor thermal crosslinking via oxidation of the cysteine residues in keratin fibers electrospun from formic acid, while Varesano and coworkers[58] investigated the effect of various temperatures (120 °C – 180 °C for up to 4 h) on the matrix stability.

The thermal treatment performed onto the Ker-PVP composite fibers did not modify their 3D network arrangements, which maintained a nanometric inter-fibers porosity (average scaffold porosity ~ 50%, as reported in Table S3). The matrices treated for 3 h (Figure S3d-f) and 5 h (Figure 2g-i) appeared to have slightly larger average diameters and wider size distributions (389 ± 129 nm and 289 ± 83 nm, respectively). This outcome can be most likely ascribed to distinct fiber depositions carried out under different environmental conditions.

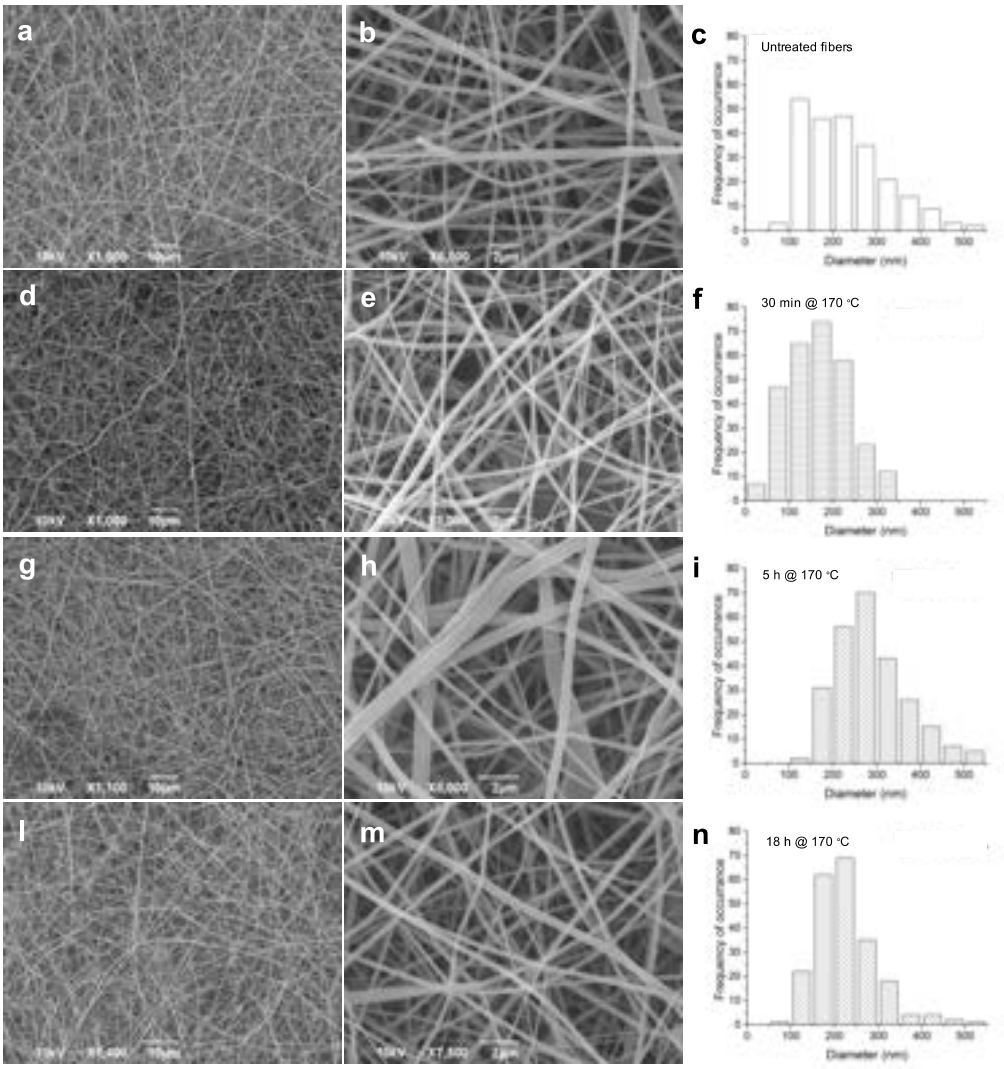

Figure 2. The thermal treatment of the composite fibers does not affect their 3D network. SEM micrographs and diameter distributions of Ker-PVP fibers as spun (a-c) or treated at 170 °C for 30 minutes (d-f), 5 h (g-i), and 18 h (l-n).

Table 1. Average diameters of the Ker-PVP fibers under study. The results are expressed as average ± standard deviation.

Sample	***Average diameter* (nm)**
Ker – PVP Untreated fibers	227 ± 94
Ker – PVP @ 170 °C for 30 min	167 ± 68
Ker – PVP @ 170 °C for 5 h	289 ± 83
Ker – PVP @ 170 °C for 18 h	222 ± 69

3.3 Chemical characterization of the keratin-PVP fibers

The effect of the thermal curing on the chemical composition of Ker-PVP nanofibers was characterized by ATR-FTIR spectroscopy (Figure 3). Comparisons with pure PVP fibers and pure keratin material were also conducted. Figure 3a shows the infrared spectra of such materials before and after the thermal curing. Main bands found in the infrared spectrum of the pristine PVP fibers were: O-H stretching mode at 3399 cm^{-1}, asymmetric and symmetric CH_2 stretching mode at 2953 and 2886 cm^{-1}, respectively, C=O stretching mode at 1653 cm^{-1}, C-N stretching mode at 1018 cm^{-1}, out-of-plane C-H bending mode at 841 cm^{-1}, and C-H rocking mode at 733 cm^{-1}. [47] After thermal curing, new peaks were observed: symmetric and asymmetric imide C=O stretching modes at 1769 and 1694 cm^{-1}, respectively, (see the top of Figure 3b) and asymmetric C-N stretching mode at 1213 cm^{-1}. This spectral profile has been previously reported for the oxidation of pyrrolidone rings

into succinimide rings in presence of UV irradiation and peroxide solutions.[59] During a thermal treatment in the presence of an oxidative atmosphere (air) and high temperatures (170 °C), a similar result is expected, as proposed in Figure 3c. In addition, the crosslinking between PVP chains through other oxygen-containing functional groups is also possible, similarly to other oxidative processes described in literature.[59] This could explain the insolubility of PVP after the thermal treatment. On the other hand, the pristine, extracted keratin material is characterized by the following absorptions: amide A at 3281 cm^{-1}, amide B at 3071 cm^{-1}, asymmetric and symmetric CH_2 stretching mode at 2922 and 2853 cm^{-1}, respectively, amide I at 1643 cm^{-1}, amide II at 1528 cm^{-1}, and amide III at 1204 cm^{-1}.[17] After thermal curing, the protein spectra revealed two new bands, assigned as follows: C=O and C-O-C stretching modes of esters at 1721 and 1142 cm^{-1}, respectively. This could indicate a condensation between hydroxyl and carboxylic groups of keratins to produce ester bonds, as proposed in Figure 3c. In the spectrum of Ker-PVP nanofibers, polyvinylpyrrolidone peaks overlaps with the Amide I and II keratin absorptions, due to the high Mw of its chains. However, Amide III contribution is visible in the composite. The thermal curing induced the same PVP oxidation and keratin condensation discussed above, although other chemical modifications and the eventual molecular interactions between both macromolecules should also be considered. The O-H band centred around at 3300 cm^{-1} shows that Ker-PVP fibers undergo a loss of water within the first 30 minutes of the treatment, since the area underneath the band diminishes significantly (Figure S4).

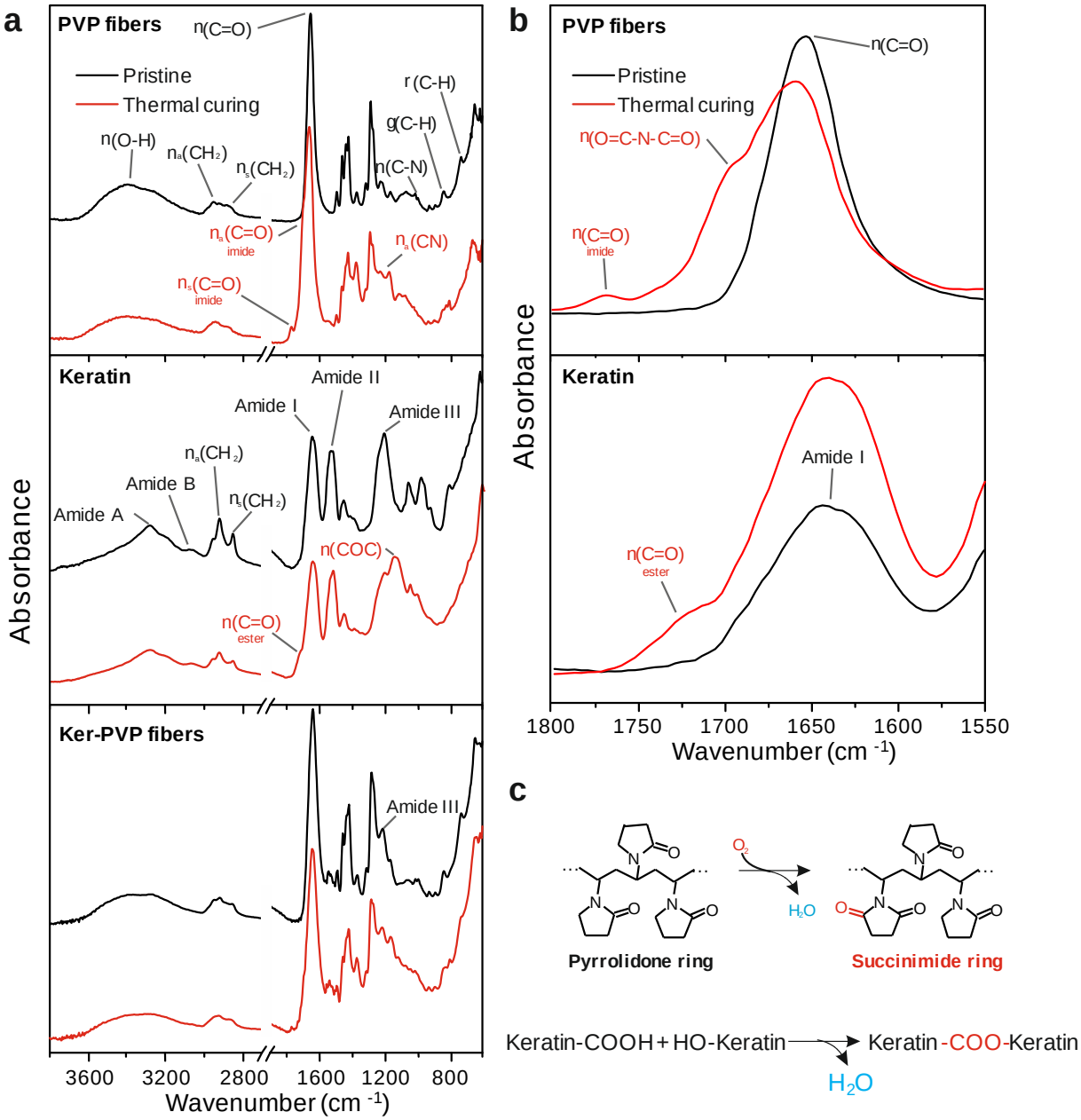

Figure 3. Keratin-PVP composite fibers response to the thermal treatment. (a) ATR-FTIR spectra of pure PVP, keratin, and Ker-PVP samples before (black) and after (red) thermal curing. The assignment of the main peaks is included. (b) ATR-FTIR spectra in the C=O region of PVP and keratin before (black) and after (red) thermal curing. (c) Proposed chemical reaction produced during the thermal curing.

3.4 Thermomechanical behavior of the keratin-PVP fibers

Figure 4a-b reports the TGA profiles of the Ker-PVP biocomposite fibers, recorded in a non-inert atmosphere. Three major steps of degradation can be identified. A first weight loss of about 3 – 5% occurs between 60 – 70 ºC, due to the adsorbed water evaporation. Even though minimal, the variation amongst the analyzed samples it is noticeable, and it reflects the effect of the thermal curing on the matrix hydroscopic behavior. The second step between 190 – 213 ºC can be ascribed to the denaturation of the α-helix protein domains within the composite fibers, in accordance with previous studies, where information on keratin secondary structure changes were obtained via Differential Scanning Calorimetry and correlated to the temperature variations.[6,58,60] As visible in Figure 4b, this degradation starts at 190 ºC for the untreated matrices, while it is triggered at higher temperatures (201 ºC and 213 ºC) for the oven-cured fibers. When reaching 340 – 345 ºC, all the samples degrade, and further temperature increases lead to the material carbonization.[51] These results indicate a greater thermal stability of the crosslinked matrices, which might be ascribed to the formation of rigid structures (such as succinimide rings) and condensed domains within the composite fibers, as hypothesized from the ATR-FTIR analysis (Figure 3c).

When designing a scaffold for tissue regeneration, the mechanical properties should be adequate for the target tissue/organ, to obtain the necessary compliance during the growth process. The Ker-PVP electrospun matrices can be tuned via thermal curing to modulate their rigidity and tensile strength. As expected, an inverse correlation between the Young's Modulus and the maximum elongation at break with respect to the curing time is evident in Figure 4c. It is important to mention that measurements were conducted at room temperature and in air, as a wet environment might slightly modify the fibers behavior. Untreated fibers can elongate up to (41 ± 7) % and sustain an ultimate stress (UTS) of 1.25 MPa, while matrices crosslinked for 18 h only

extend up to (27 ± 4) % with a 3-fold increase in their tensile strength and apparent Young's modulus (Table S4). Similar values were obtained for keratin/PVA blend electrospun fibers in terms of Young's modulus[40] and UTS/elongation.[61,34] The changes in ductility can be visualized on the SEM micrographs of the fracture borders reported in Figure 4d-g. After reaching the breaking point, the untreated matrices (Figure 4d) appeared more elongated and stretched, as their fibers have been almost teared apart during the tensile experiment. When subjected to longer thermal treatments, the network responded with more fragile fibers, which did not undergo any visible deformation nor alignment along the test axis (Figure 4c-d). Thanks to the structure and chemical composition of the protein-based composite, by acting on the thermal treatment duration a range of mechanical properties can be potentially achieved. Beside the mechanical integrity and compliance, compelling for the success of a biomaterial scaffold is its capacity to withstand abrupt morphological and structural changes when in contact with a water-like milieu.

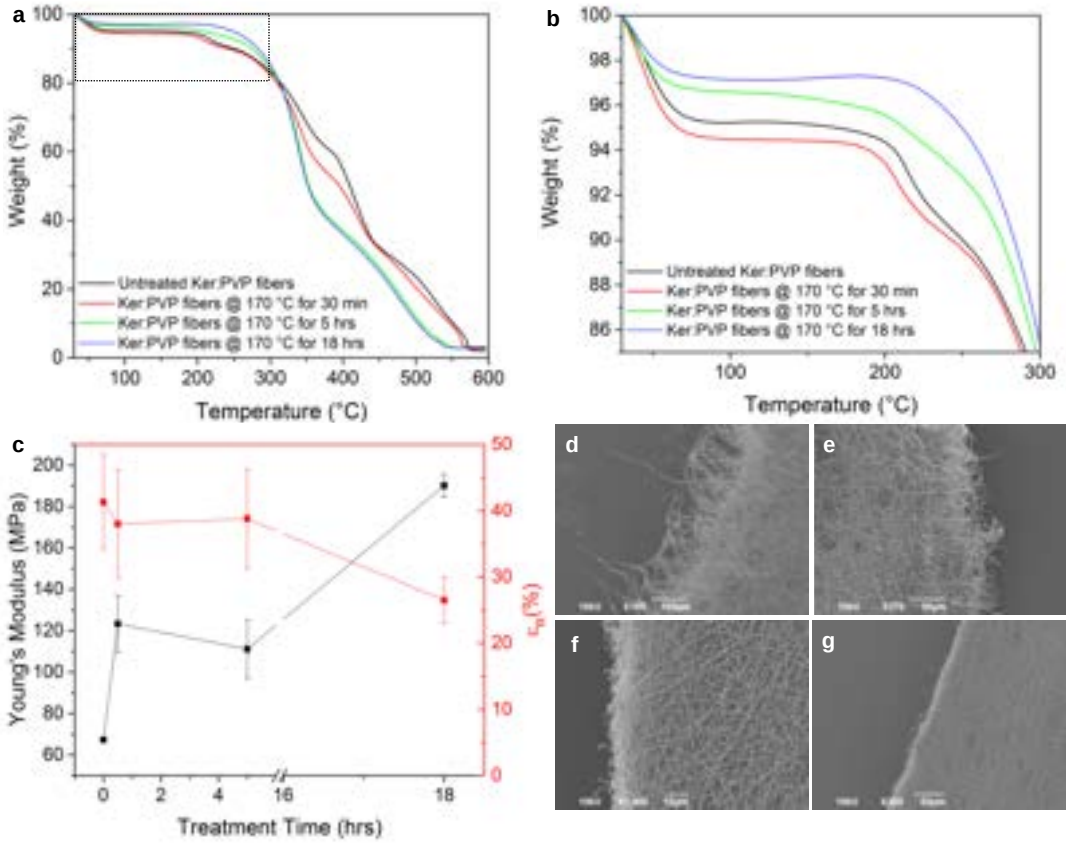

Figure 4. The thermal treatment of the composite fibers stabilizes the composite network and improves its mechanical resistance. TGA measurements: weight loss vs. Temperature (a, b). Young's Modulus and elongation at break variations with respect to the thermal treatment duration (c); SEM micrographs of the fracture edges for the untreated matrices (d), and Ker-PVP fibers treater at 170 °C for 30 minutes (e), 5 h (f), and 18 h (g).

3.5 Keratin-PVP fibers response to a wet environment

The investigation of the Ker-PVP matrices stability when in contact with a wet environment was carried out by assessing the water vapor uptake, the water contact angle, and the morphological changes (Figure 5). All these aspects are crucial for the envisioned biological application, as cells require a hydrophilic and structurally stable surrounding to attach onto. Aside

from strengthening their thermomechanical stability under dry conditions, the thermal treatment performed onto the Ker-PVP matrices also influenced their capability to absorb moisture (Figure 5a and Table S5). In fact, when incubated in a 100% R.H. chamber the untreated fibers increased by 53.2% their initial weight, while a decreasing trend was observed for the cured protein fibers. As a fallout of the interactions between the water molecules and the polypeptide domains or the PVP polymeric chains, moisture could potentially modify the scaffold physico-chemical characteristics, thus impairing its storage life. As expected, the thermal treatment appears to further stabilize the protein-based biocomposite matrices.

Providing physical cues for cell attachment, wettability greatly affects the cell-material interaction and can dictate the success of the designed scaffold. Both keratin and PVP are hydrophilic materials, that can quickly undergo dissolution upon contact with water. Water contact angle measurements onto self-standing fibrous matrices (average thickness of 450 μm ca.) were carried out via sessile-drop method. Due to the presence of a highly porous network, the water drops were rapidly penetrating into the structure to be absorbed by the matrix within a few seconds. This behavior was observed for all the samples, indicating that the performed thermal curing did not considerably affect the wettability of the protein-based scaffolds.

To assess the structural integrity of the membranes when soaked in a water-like medium, the fibers were immersed for 24 h in PBS (pH 7.4) and, subsequently, observed under the SEM. Untreated matrices and fibers cured for only 30 minutes immediately dissolved upon immersion in the buffer, and the visualization was only possible for the composite fibers treated for 5 h (Figure 5b-c) and 18 h (Figure 5d-e). The 5 h treatment was not sufficient to prevent the collapse of the fibrous structure: the partially dissolved material contributed to glue together the network, and filaments of different dimensions became distinguishable in the degraded film-like matrix. By

extending the curing time up to 18 h, the nanofibrous 3D arrangement was retained, and the fibers, although homogeneous in their sizes, revealed a slightly swollen morphology. A similar variation in the morphology was observed by Edwards *et al.*[43] and others.[49,58,62] Aluigi *et al.*[17] have hypothesized that a crosslinking between the amino acids side chains of thermally treated pure keratin fibers, electrospun from formic acid solutions, could be responsible for their increased water stability. In the case of our composite matrices, esterification and condensation reactions within the keratin domains or between the protein and the PVP polymeric chains could also be considered (Figure 3c).

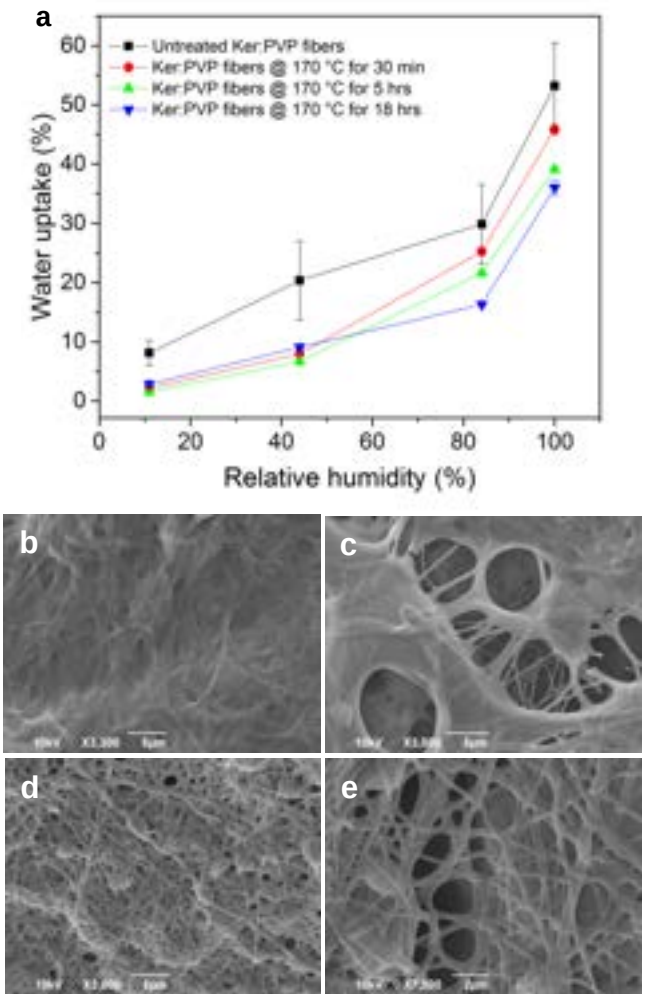

Figure 5. Keratin-based fibers response to a wet environment. (a) Water vapor uptake results (given as %) of the Ker-PVP fibrous matrices, either pristine or thermally treated. SEM micrographs of Ker-PVP fibers treated at 170 °C for 5 h (b-c) or 18 h (d-e) and immersed in PBS (pH 7.4, room Temperature) overnight. With longer thermal crosslinking, the 3D fibrous network of the electrospun matrices is preserved.

To support the restoration of tissue physiological functions, a scaffold biomaterial should gradually degrade, in order to provide the necessary mechanical substratum for the new tissue formation, while allowing nutrients exchange and cell infiltration.[63] Multiple challenges reside in the scaffold design and in its components' choice, both critical in dictating the degradation profile. To simulate the *in vivo* proteolytic degradation conditions, the Ker-PVP matrices, which preserved their structure after a 24-h incubation in PBS, were subjected to Protease XIV from *Streptomyces griseus* for two weeks. This serine protease cleaves the protein macromolecules at different locations[63] and it has been shown to predominantly degrade exposed amorphous regions.[64] The biodegradation experiment protocol has been adapted from previous studies, where Protease XIV was used for silk[63–66], and keratin[35] based hydrogels and nanofibers. The enzyme destructive activity towards the morphology of the electrospun Ker-PVP matrices is visible with the SEM micrographs in Figure 6. Up to 3 days of incubation, the fibers were distinguishable, although partially collapsed, and pores/voids were still present (yellow arrows in Figure 6b, c). After 5 days of biodegradation, the swollen fibers appeared to fuse and glue together to form flatter structures (red arrows in Figure 6d). Between day 5 and 7 of proteolytic digestion, the weight loss dropped to 85.8 ± 2.3 (Table 2) and the matrix lost its 3D network arrangement. Finally, after 14 days, the structure is completely collapsed in a film-like morphology (Figure 6f) and the weight loss reached 75.8 ± 0.9 (Table 2).

Taken together, these results suggest that the Ker-PVP fibers treated at 170 °C for 18 h remained stable under various environmental conditions, were highly hydrophilic when in contact with water, and kept preserved the 3D fibrous network morphology up to 5 days when incubated in an enzyme-containing media, thus providing the most suitable platform for cell attachment and growth.

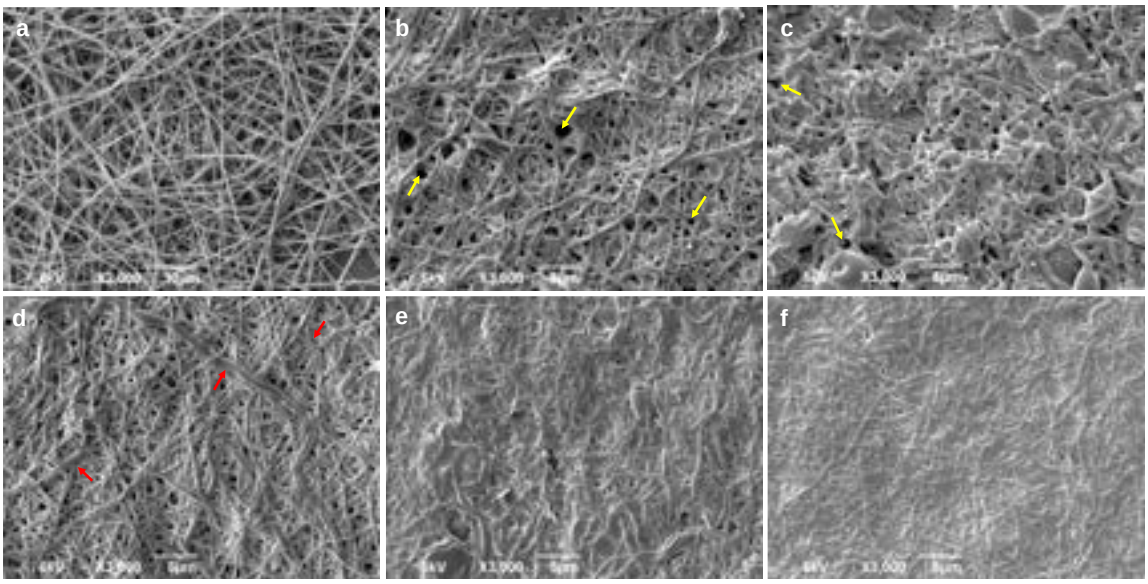

Figure 6. Keratin-based fibers resisted to the enzymatic degradation. SEM micrographs of Ker-PVP matrices (170 °C for 18 h) before (a) and after immersion in a buffer containing Protease XIV from *Streptomyces griseus*. The assay was carried out for up to 14 days and images from reference samples were obtained at 1 (b), 3 (c), 5 (d), 7 (e), and 14 (f) days of incubation. Yellow arrows in (b) and (c) indicate the presence of hollow structures in between of collapsed fibers. Red arrows in (d) highlight how several fibers started to glue together after 5 days of protease digestion.

Table 2. Weight loss (given as %) of the Ker-PVP fibrous matrices (thermally treated for 18 h) as result of the enzymatic degradation in the presence of Protease XIV. Data are expressed as average ± standard deviation.

Sample	***Day 1***	***Day 3***	***Day 5***	***Day 7***	***Day 14***
Ker – PVP @ 170 °C for 18 h	*99.7 ± 0.5*	*99.5 ± 0.5*	*97.6 ± 0.9*	*85.8 ± 2.3*	*75.8 ± 0.9*

3.6 Keratin-PVP fibers biocompatibility and suitability for cell support

Cell viability of the Ker-PVP fibers cured for 18 h at 170 °C was assessed using primary human dermal fibroblast adult cells (HDFa) at passages P3-P6, and primary human epidermal keratinocyte adult (HEKa) cells at passages P4-P5. Following the ISO10993-5:2009 norm, the matrices were incubated overnight in cell culture medium under sterile conditions, and the extract was used to assess indirect cytotoxicity. As visible from the MTS data reported in Figure 7a and in Figure S5 (Supporting Information), the released residues presented good cytocompatibility, with a slightly increasing trend between 24 and 48 h of incubation, similar to what observed by Yen *et al.*[27] Confocal imaging investigation conducted onto HDFa cells revealed an elongated and spread out morphology, characterized by well-defined and stretched actin filaments, indicative of healthy fibroblasts, comparable with the control cells (Figure 7b, c).

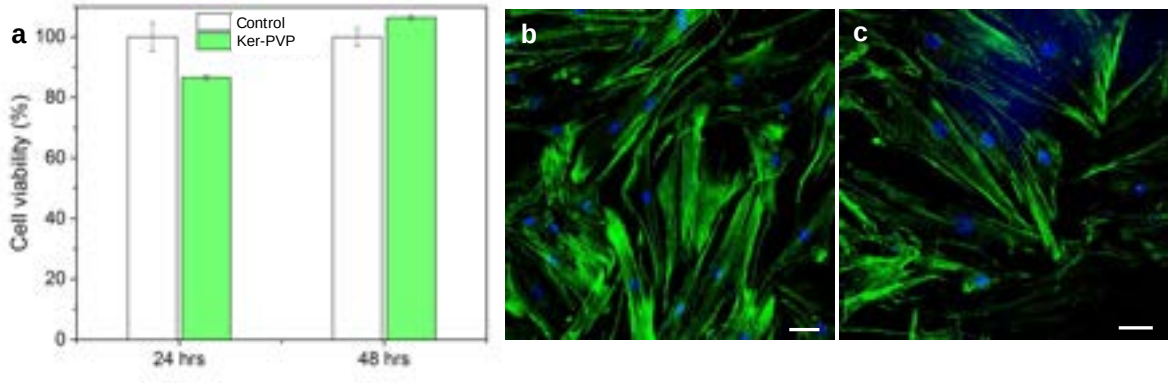

Figure 7. Keratin-based fibers did not hinder primary human fibroblasts viability. (a) Cell viability results (MTS assay) and (b, c) confocal images of primary HDFa cells cultured for up to 48 h in the presence of Ker-PVP fibers (170 °C for 18 h) extraction media. Control cells treated with plain culture media are depicted in (b). Scale bar 50 μm.

Wool keratinous fractions have been shown to present cell adhesion peptide motifs, such as arginine – glycine – aspartic acid (RGD) and leucine – aspartic acid – valine (LDV),[7,19,50] recognized by the $\alpha_4\beta_1$ integrin binding sequence expressed at the cell membrane of various cell types. These sequences are able to trigger some of the intracellular signaling pathways involved in cellular attachment and tissue growth.[28,67] In this study, primary human dermal fibroblasts were directly plated onto thermally cross-linked Ker-PVP biocomposite nanofibers, to investigate their ability to promote cell adhesion and proliferation. Thanks to their preserved 3D network of nanometric fibers (average diameter ~ 222 nm – Table 1) and nanometric inter-fibrous porosity, the cured matrices constituted a favorable environment for cell spreading (Figure 8, Figure S5) and attachment (Figure 9, Figure S6). After 72 h of culture, many well spread-out primary fibroblasts adhered to the matrix, following the ridged curvature of the surface (Figure 8e, f), indicating a good cell-material interaction and a stabilized interface.

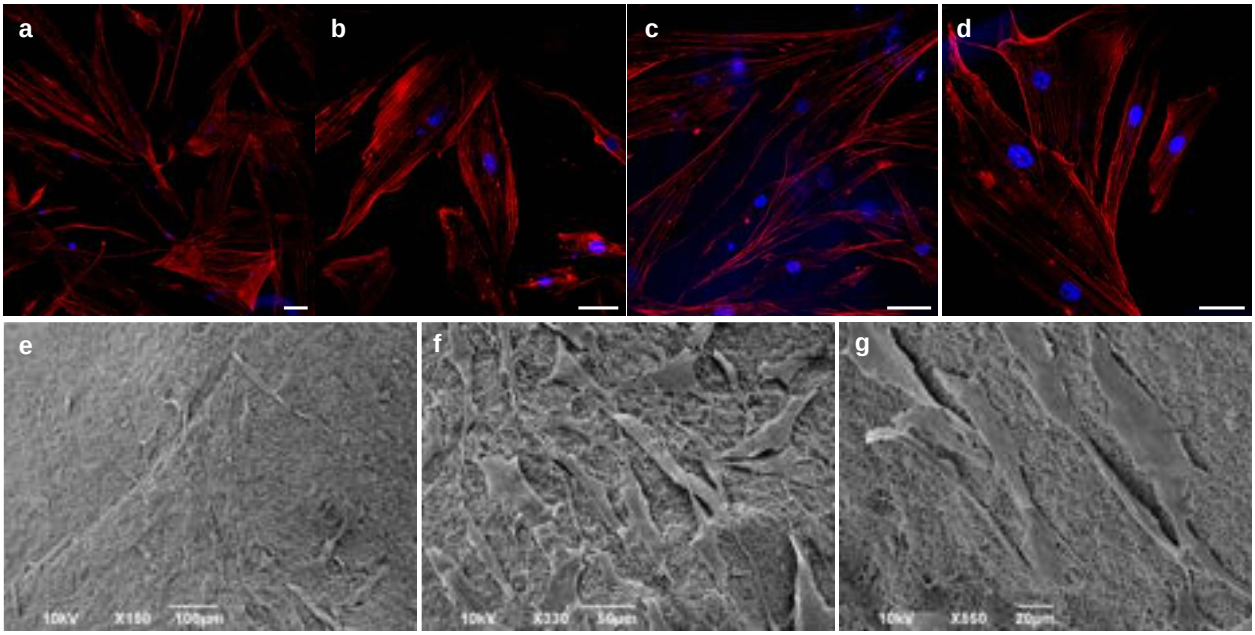

Figure 8. Keratin-based fibers are suitable for primary human cell seeding. Confocal images of primary HDFa cells plated onto Ker-PVP fibers (170 °C for 18 h) and cultured for 3 days (a-d). Nuclei, stained with DAPI, are highlighted in blue, while the actin fibers are shown in red (Alexa Fluor Phalloidin 546). Scale bar 50 μm. SEM micrographs of the cultured fibroblasts (e-g), revealing a good cell spreading and attachment onto the 3D fibrous network.

From the lamellopodia at the leading edges of the cell membrane, numerous filopodia are extending, as highlighted in Figure 9. These cytoplasmic projections sense the substrate and are responsible for the formation of the focal adhesion points, crucial for cell survival and migration. The SEM imaging investigation clearly revealed how the fibroblasts were able to integrate within the surrounding keratin-based matrices, as the filopodia elongated from the membrane to entangle with the fibers in their proximity (Figure 9c, d – white arrows; Figure S6b, d – white arrows). Future strategies to increase the scaffold porosity either based on the change in the deposition parameters or in the matrices post-processing[68] would be considered to promote cell infiltration. Considering the delicate primary culture used for the *in vitro* biocompatibility assessment, our results further support the strong potentialities of the thermally cured Ker-PVP as scaffold for skin tissue regeneration.

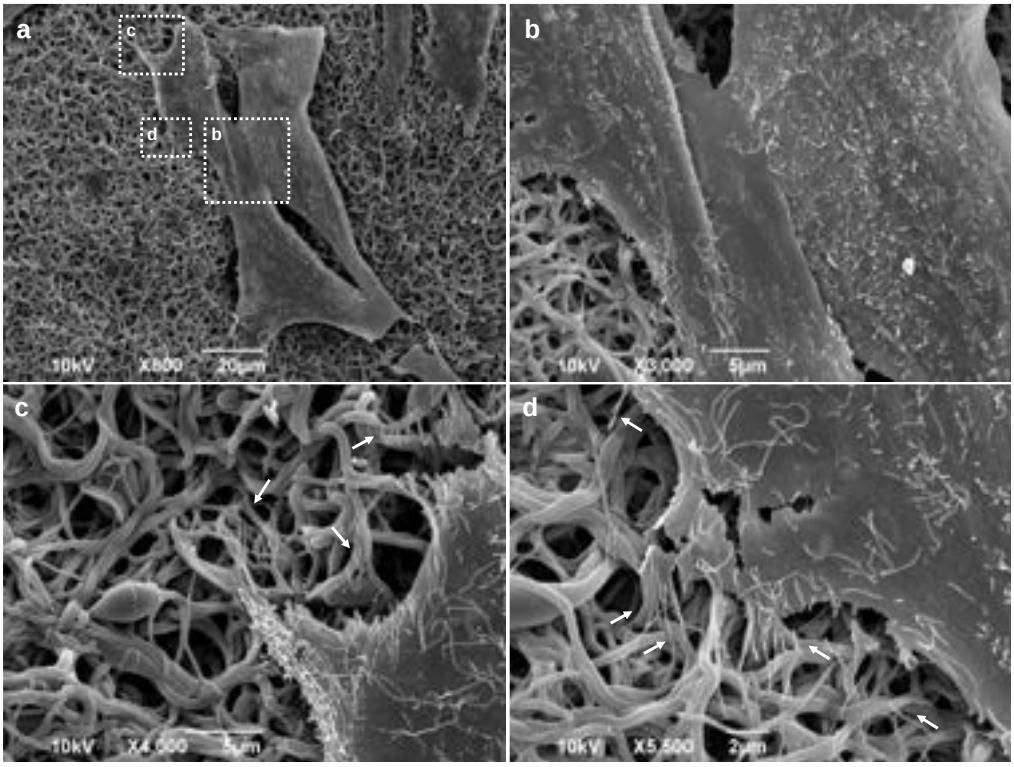

Figure 9. Primary human fibroblasts extend their filopodia within the 3D keratin-based network. SEM micrographs of fibroblasts cultured for 3 days onto Ker-PVP fibers (170 °C for 18 h). Insets: (b) cell-to-cell interactions; (c) zoom of the migration front zone, (d) zoom revealing the cell attachment. Filopodia extending within the fibrous matrices are indicated with white arrows.

4. Conclusions

Alternative ways of biomass disposal call for the development of novel biocomposites fabricated according to more sustainable and cost-effective approaches. These strategies may be of potential interest in various biomedical and industrial settings (*e.g.* wound management, disposable gauze fabrication). In this study, wool fibers from textile industry were used as source of keratins for skin tissue regeneration substrates. By combining for the first time the extracted

wool keratins with PVP as adjuvant polymer, homogenous nanofibers were obtained with an all-water co-electrospinning process. Various thermal treatments were performed to stabilize the fibrous 3D network and prevent the immediate dissolution upon contact with a water-like milieu. In addition, by acting on the treatment duration, thermomechanical properties, sensitivity to moisture and enzymatic degradation resistance could be enhanced. This is crucial to improve the scaffold handling and storage-ability, in an effort of designing practical and stable ECM-like constructs for tissue engineering applications. The intrinsic hydrophilic nature of both the protein and the adjuvant polymer were not undermined, and the thermally cured Ker-PVP matrices constituted a suitable environment for primary human dermal fibroblasts attachment and spreading, also demonstrating biocompatibility towards primary human epidermal keratinocytes. More strikingly, the choice of these human primary cellular models for the *in vitro* validation provided a more predictive outcome for the envisioned tissue engineering application. Overall, our proposed protein-based fibers represent a promising platform for the design of skin scaffolds from renewable resources. Future modifications of the components formulation to increase the protein content, the loading of active agents in the co-spinning process (*e.g.* anti-oxidant, anti-bacterial compounds, growth factors), and the design of an integrated keratin hydrogel / Ker-PVP fibers system presenting differential porosity would allow an additional tuning of the physico-chemical properties and a further functionalization of our biocomposites to support the skin tissue regeneration process throughout its various steps.

Notes

The authors declare no competing financial interest.

This research did not receive any specific grant from funding agencies in the public, commercial, or not-for-profit sectors.

CRediT Author Statement

Giulia Suarato: conceptualization, investigation, visualization, validation, writing – original draft, writing – review & editing; *Marco Contardi*: investigation, validation; writing – review & editing; *Giovanni Perotto*: validation, resources; *Jose'-Alejandro Heredia-Guerrero*: investigation, visualization, and writing (FT-IR); *Fabrizio Fiorentini*; investigation (keratinocyte *in vitro* experiments); *Luca Cesaracciu*: investigation (mechanical tests); *Cataldo Pignatelli*: investigation (gel-electrophoresis); *Doriana Debellis*: investigation (SEM staining sample preparation); *Rosalia Bertorelli*: supervision; *Athanassia Athanassiou*: supervision, writing – original draft.

Acknowledgment

The authors would like to thank Lara Marini for her help with the TGA measurement acquisition and Dr. Michele Oneto for the interesting discussions about the confocal spectral unmixing.

References

1 N. H. C. S. Silva, C. Vilela, I. M. Marrucho, C. S. R. Freire, C. Pascoal Neto and A. J. D. Silvestre, *J. Mater. Chem. B*, 2014, **2**, 3715–3740.

2 G. Suarato, R. Bertorelli and A. Athanassiou, *Front. Bioeng. Biotechnol.*, 2018, **6**, 1–11.

3 S. Sharma and A. Gupta, *Brazilian Arch. Biol. Technol.*, 2016, **59**, e16150684.

4 K. Chojnacka, H. Górecka, I. Michalak and H. Górecki, *Waste and Biomass Valorization*, 2011, **2**, 317–321.

5 C. Ferroni, G. Sotgiu, A. Sagnella, G. Varchi, A. Guerrini, D. Giuri, E. Polo, V. T. Orlandi, E. Marras, M. Gariboldi, E. Monti and A. Aluigi, *Biomacromolecules*, 2016, **17**, 2882–2890.

6 J. Fan, T. Da Lei, J. Li, P. Y. Zhai, Y. H. Wang, F. Y. Cao and Y. Liu, *Mater. Des.*, 2016, **104**, 60–67.

7 L. Sando, M. Kim, M. L. Colgrave, J. A. M. Ramshaw, J. A. Werkmeister and C. M. Elvin, *J. Biomed. Mater. Res. - Part A*, 2010, **95**, 901–911.

8 B. Wang, W. Yang, J. McKittrick and M. A. Meyers, *Prog. Mater. Sci.*, 2016, **76**, 229–318.

9 P. Hill, H. Brantley and M. Van Dyke, *Biomaterials*, 2010, **31**, 585–593.

10 I. Sinkiewicz, A. Śliwińska, H. Staroszczyk and I. Kołodziejska, *Waste and Biomass Valorization*, 2017, **8**, 1043–1048.

11 C. Tonin, M. Zoccola, A. Aluigi, A. Varesano, A. Montarsolo, C. Vineis and F. Zimbardi, *Biomacromolecules*, 2006, **7**, 3499–3504.

12 P. Bhavsar, M. Zoccola, A. Patrucco, A. Montarsolo, R. Mossotti, G. Rovero, M. Giansetti and C. Tonin, *ACS Sustain. Chem. Eng.*, 2016, **4**, 6722–6731.

13 Z. Zhang, Y. Nie, Q. Zhang, X. Liu, W. Tu, X. Zhang and S. Zhang, *ACS Sustain. Chem. Eng.*, 2017, **5**, 2614–2622.

14 A. Shavandi, T. H. Silva, A. A. Bekhit and A. E. D. A. Bekhit, *Biomater. Sci.*, 2017, **5**, 1699–1735.

15 S. Rahayu, S. D and M. Thenawidjaja Suhartono, *Biocatal. Agricaltural Biotecnol.*, 2012, **1**, 152–158.

16 T. R. Ham, R. T. Lee, S. Han, S. Haque, Y. Vodovotz, J. Gu, L. R. Burnett, S. Tomblyn and J. M. Saul, *Biomacromolecules*, 2016, **17**, 225–236.

17 A. Aluigi, A. Corbellini, F. Rombaldoni, M. Zoccola and M. Canetti, *Int. J. Biol. Macromol.*, 2013, **57**, 30–37.

18 A. Patrucco, F. Cristofaro, M. Simionati, M. Zoccola, G. Bruni, L. Fassina, L. Visai, G. Magenes, R. Mossotti, A. Montarsolo and C. Tonin, *Mater. Sci. Eng. C*, 2016, **61**, 42–50.

19 V. Verma, P. Verma, P. Ray and A. R. Ray, *Biomed. Mater.*, 2008, **3**, 025007

20 L. Liu, W. Yuan and J. Wang, *Biomech. Model. Mechanobiol.*, 2010, **9**, 659–70.

21 H. Mori and M. Hara, *Mater. Sci. Eng. C*, 2018, **91**, 19–25.

22 C. H. Yao, C. Y. Lee, C. H. Huang, Y. S. Chen and K. Y. Chen, *Mater. Sci. Eng. C*, 2017, **79**, 533–540.

23 S. Xu, L. Sang, Y. Zhang, X. Wang and X. Li, *Mater. Sci. Eng. C*, 2013, **33**, 648–655.

24 M. Park, H. K. Shin, B. S. Kim, M. J. Kim, I. S. Kim, B. Y. Park and H. Y. Kim, *Mater. Sci. Eng. C*, 2015, **55**, 88–94.

25 C. W. Lin, Y. K. Chen, K. C. Tang, K. C. Yang, N. C. Cheng and J. Yu, *J. Tissue Eng.*

Regen. Med., 2019, **13**, 1044–1058.
26 K. Yamauchi, H. Hojo, Y. Yamamoto and T. Tanabe, *Mater. Sci. Eng. C*, 2003, **23**, 467–472.
27 K. C. Yen, C. Y. Chen, J. Y. Huang, W. T. Kuo and F. H. Lin, *J. Mater. Chem. B*, 2015, **4**, 237–244.
28 P. Sierpinski, J. Garrett, J. Ma, P. Apel, D. Klorig, T. Smith, L. A. Koman, A. Atala and M. Van Dyke, *Biomaterials*, 2008, **29**, 118–128.
29 V. Bailey, E. Fearing, E. Mark and V. Dyke, *Acta Biomater.*, 2014, **10**, 3136–3144.
30 T. Posati, D. Giuri, M. Nocchetti, A. Sagnella, M. Gariboldi, C. Ferroni, G. Sotgiu, G. Varchi, R. Zamboni and A. Aluigi, *Eur. Polym. J.*, 2018, **105**, 177–185.
31 J. M. Saul, M. D. Ellenburg, R. C. De Guzman and M. Van Dyke, *J. Biomed. Mater. Res. - Part A*, 2011, **98 A**, 544–553.
32 S. Sadeghi, J. Nourmohammadi, A. Ghaee and N. Soleimani, *Int. J. Biol. Macromol.*, 2020, **147**, 1239–1247.
33 M. I. Bajestani, S. Kader, M. Monavarian, S. M. Mousavi, E. Jabbari and A. Jafari, *Int. J. Biol. Macromol.*, 2020, **142**, 790–802.
34 P. Naderi, M. Zarei, S. Karbasi and H. Salehi, *Eur. Polym. J.*, 2020, **124**, 109502.
35 D. Giuri, M. Barbalinardo, G. Sotgiu, R. Zamboni, M. Nocchetti, A. Donnadio, F. Corticelli, F. Valle, C. G. M. Gennari, F. Selmin, T. Posati and A. Aluigi, *Nanoscale*, 2019, **11**, 6422–6430.
36 G. Perotto, G. Sandri, C. Pignatelli, G. Milanesi and A. Athanassiou, *J. Mater. Chem. B*, 2019, **7**, 4385–4392.
37 J. Yuan, J. Geng, Z. Xing, K.-J. Shim, I. Han, J. Kim, I.-K. Jang and J. Shen, *J Tissue Eng Regen Med*, 2015, **9**, 1027–1035.
38 S. Singaravelu, G. Ramanathan, T. Muthukumar, M. D. Raja, N. Nagiah, S. Thyagarajan, A. Aravinthan, P. Gunasekaran, T. S. Natarajan, G. V. N. Geetha Selva, J. H. Kim and U. T. Sivagnanam, *J. Mater. Chem. B*, 2016, **4**, 3982–3997.
39 A. Aluigi, C. Vineis, A. Varesano, G. Mazzuchetti, F. Ferrero and C. Tonin, *Eur. Polym. J.*, 2008, **44**, 2465–2475.
40 J. Choi, G. Panthi, Y. Liu, J. Kim, S. H. Chae, C. Lee, M. Park and H. Y. Kim, *Polymer (Guildf).*, 2015, **58**, 146–152.
41 S. Li and X. H. Yang, *Adv. Mater. Sci. Eng.*, 2014, **2014**, ID 163678.
42 J. Li, Y. Li, L. Li, A. F. T. Mak, F. Ko and L. Qin, *Polym. Degrad. Stab.*, 2009, **94**, 1800–1807.
43 A. Edwards, D. Jarvis, T. Hopkins, S. Pixley and N. Bhattarai, *J. Biomed. Mater. Res. - Part B Appl. Biomater.*, 2015, **103**, 21–30.
44 Y. Li, Y. Wang, J. Ye, J. Yuan and Y. Xiao, *Mater. Sci. Eng. C*, 2016, **68**, 177–183.
45 J. Dou, Y. Wang, X. Jin, P. Li, L. Wang, J. Yuan and J. Shen, *Mater. Sci. Eng. C*, 2020, **107**, 110246.
46 M. Contardi, D. Russo, G. Suarato, J. A. Heredia-Guerrero, L. Ceseracciu, I. Penna, N. Margaroli, M. Summa, R. Spanò, G. Tassistro, L. Vezzulli, T. Bandiera, R. Bertorelli, A. Athanassiou and I. S. Bayer, *Chem. Eng. J.*, 2019, **358**, 912–923.
47 M. Contardi, J. A. Heredia-Guerrero, G. Perotto, P. Valentini, P. P. Pompa, R. Spanò, L. Goldoni, R. Bertorelli, A. Athanassiou and I. S. Bayer, *Eur. J. Pharm. Sci.*, 2017, **104**, 133–144.
48 X. Y. Dai, W. Nie, Y. C. Wang, Y. Shen, Y. Li and S. J. Gan, *J. Mater. Sci. Mater. Med.*,

2012, **23**, 2709–2716.
49 J. W. Kim, M. J. Kim, C. S. Ki, H. J. Kim and Y. H. Park, *Int. J. Biol. Macromol.*, 2017, **105**, 541–548.
50 J. R. Richter, R. C. De Guzman, O. K. Greengauz-Roberts and M. Van Dyke, *Acta Biomater.*, 2012, **8**, 274–281.
51 V. Agarwal, A. G. Panicker, S. Indrakumar and K. Chatterjee, *Int. J. Biol. Macromol.*, 2019, **133**, 382–390.
52 A. Aluigi, C. Tonetti, C. Vineis, C. Tonin and G. Mazzuchetti, *Eur. Polym. J.*, 2011, **47**, 1756–1764.
53 C. A. Schneider, W. S. Rasband and K. W. Eliceiri, *Nat. Methods*, 2012, **9**, 671–675.
54 A. C. Cassoni, R. Freixo, A. I. E. Pintado, M. Amorim, C. D. Pereira, A. R. Madureira and M. M. E. Pintado, *ACS Sustain. Chem. Eng.*, 2018, **6**, 12268–12274.
55 H. Xu and Y. Yang, *ACS Sustain. Chem. Eng.*, 2014, **2**, 1404–1410.
56 A. Varesano, A. Aluigi, C. Vineis and C. Tonin, *J. Polym. Sci. Part B Polym. Phys.*, 2008, **46**, 1193–1201.
57 M. A. D. Boakye, N. P. Rijal, U. Adhikari and N. Bhattarai, *Materials (Basel).*, 2015, **8**, 4080–4095.
58 A. Varesano, C. Vineis, C. Tonetti, D. O. S. Ramírez and G. Mazzuchetti, *J. Appl. Polym. Sci.*, 2014, **131**, 40532.
59 X. Zhu, P. Lu, W. Chen and J. Dong, *Polymer (Guildf).*, 2010, **51**, 3054–3063.
60 M. Zoccola, A. Aluigi and C. Tonin, *J. Mol. Struct.*, 2009, **938**, 35–40.
61 M. He, B. Zhang, Y. Dou, G. Yin, Y. Cui and X. Chen, *RSC Adv.*, 2017, **7**, 9854–9861.
62 P. Wu, X. Dai, K. Chen, R. Li and Y. Xing, *Int. J. Biol. Macromol.*, 2018, **114**, 1168–1173.
63 R. L. Horan, K. Antle, A. L. Collette, Y. Wang, J. Huang, J. E. Moreau, V. Volloch, D. L. Kaplan and G. H. Altman, *Biomaterials*, 2005, **26**, 3385–3393.
64 J. Brown, C.-L. Lu, J. Coburn and D. L. Kaplan, *Acta Biomater.*, 2015, **11**, 212–221.
65 C. Pignatelli, G. Perotto, M. Nardini, R. Cancedda, M. Mastrogiacomo and A. Athanassiou, *Acta Biomater.*, 2018, **73**, 365–376.
66 J. A. Kluge, A. Thurber, G. G. Leisk, D. L. Kaplan and A. Luis Dorfmann, *J. Mech. Behav. Biomed. Mater.*, 2010, **3**, 538–547.
67 S. Wang, F. Taraballi, L. P. Tan and K. W. Ng, *Cell Tissue Res.*, 2012, **347**, 795–802.
68 J. M. Ameer, P. R. Anil Kumar and N. Kasoju, *J. Funct. Biomater.*, 2019, **10**, 1–21.